Modeling and Analysis of DC Microgrids as Stochastic Hybrid Systems

Jacob A. Mueller, *Member, IEEE*, and Jonathan W. Kimball, *Senior Member, IEEE*

***Abstract*—This article proposes a method of predicting the influence of random load behavior on the dynamics of dc microgrids and distribution systems. This is accomplished by combining stochastic load models and deterministic microgrid models. Together, these elements constitute a stochastic hybrid system. The resulting model enables straightforward calculation of dynamic state moments, which are used to assess the probability of desirable operating conditions. Specific consideration is given to systems based on the dual active bridge (DAB) topology. Bounds are derived for the probability of zero voltage switching (ZVS) in DAB converters. A simple example is presented to demonstrate how these bounds may be used to improve ZVS performance as an optimization problem. Predictions of state moment dynamics and ZVS probability assessments are verified through comparisons to Monte Carlo simulations.**

***Index Terms*—Dual active bridge (DAB) converter, generalized average model, stochastic hybrid system (SHS), zero voltage switching (ZVS).**

I. Introduction

MICROGRIDS have rapidly emerged as a solution for improving the flexibility and resiliency of power delivery systems. Microgrids provide a framework for integrating distributed resources in close proximity to the loads they serve. When equipped with energy storage resources, a microgrid may operate as an autonomous island decoupled from the bulk power system. Because microgrids do not, in general, require a connection to a traditional utility system, they are free to consider alternative means of power distribution [1]. An important subset of microgrids distribute power as dc instead of traditional synchronous ac. A key benefit of dc distribution is the elimination of bulky 60 Hz transformers, which reduces the weight and volume of power conversion equipment. As a result, dc distribution is an attractive solution for mobile platforms such as spacecraft, more-electric aircraft, automobiles, and electric warships [2]–[4]. Even applications that are not subject to stringent weight and volume constraints may benefit from dc distribution due to the increasing prevalence of dc-native generation sources, loads, and energy storage resources.

Like all power delivery systems, the operating state of a dc microgrid is heavily influenced by the operation of system loads. Practical loads, which are time-varying and nondeterministic, introduce uncertainty in the dynamic behavior of the microgrid system. For some analysis and design objectives, dealing with the complexity of stochastic load influences is not necessary. Stability analyses, for example, rarely include stochastic behavior. A typical approach to small-signal stability is to identify a steady-state operating point for a deterministic loading condition, linearize a system model around that operating point, and inspect the locations of the linearized model's eigenvalues [5]. The analysis relies on an approximation of loads as deterministic and constant in time, and while real-world loads fit neither of these conditions, this approach is an effective tool for evaluating the stability of both microgrids and bulk power systems.

However, deterministic models are unable to provide insights into the performance and reliability of a system over time. These sorts of assessments require quantitative descriptions of the distribution of system operating conditions over a given time range [6]. The performance of a converter depends on its operating point, and there are often operating ranges that are more desirable than others. For example, soft-switching significantly improves converter efficiency and reliability but is typically only possible for a subset of operating conditions. It is preferable to either operate the converter in its soft-switching range as often as possible or to design the soft-switching range around the typical system operating conditions. Either approach requires quantitative descriptions of expected operating conditions as a function of the behavior of loads within the system. This article focuses on developing modeling tools to generate these descriptions.

The challenge of predicting expected operating conditions as a function of uncertain load influences essentially involves two tasks: (1) building stochastic models of load behavior and (2) integrating those models into deterministic dynamic system models. Established methods for both of these tasks exist in bulk power system analysis. Load behavior in a traditional power system is commonly approximated using Gaussian processes [7], [8]. By integrating Gaussian load processes as inputs to linearized power system models (such as those employed for small-signal stability analysis), distributions of power system states can be calculated directly [9]. The justifications for using Gaussian load approximations and linearized system models

Manuscript received April 23, 2020; revised October 1, 2020 and December 13, 2020; accepted January 21, 2021. Date of publication January 28, 2021; date of current version May 5, 2021. This work was supported in part by the National Science Foundation, under Award 1406156 and in part by the U.S. Department of Energy Office of Electricity Energy Storage Program. Recommended for publication by Associate Editor J. M. Guerrero. *(Corresponding author: Jonathan Kimball.)*

Jacob A. Mueller is with Sandia National Laboratories, Albuquerque, NM 87185 USA (e-mail: jmuelle@sandia.gov).

Jonathan W. Kimball is with the Department of Electrical and Computer Engineering, Missouri University of Science and Technology, Rolla, MO 65409 USA (e-mail: kimballjw@mst.edu).

Color versions of one or more figures in this article are available at https://doi.org/10.1109/TPEL.2021.3055456.

Digital Object Identifier 10.1109/TPEL.2021.3055456

are both based on system scale [10]. Since the number of individual loads in a traditional power system is typically very high, Gaussian system-level approximations are justified by the central limit theorem. Similarly, each individual load constitutes only a small fraction of the aggregate system load, so changes in individual load behavior are generally small enough to be considered a small-signal disturbance. However, as the scale of the system decreases, the impact of an individual load device becomes more significant with respect to the total load. As a result, Gaussian approximations and linearized dynamic models become less accurate [11].

The breakdown of Gaussian load approximations is problematic for microgrids. Microgrids are, by definition, smaller in scale than traditional power systems. This is especially true for isolated microgrids on mobile platforms. System-level load behavior in a microgrid cannot be accurately approximated with Gaussian distributions and a transient load change cannot safely be considered a small-signal disturbance. Instead, load behavior is characterized by large-signal transient events, or "jumps," which occur at random intervals. This means that neither the load modeling methods nor the deterministic dynamic models from conventional power system analysis are applicable. A suitable approach to predicting expected system operating conditions must be compatible with discrete jump events representing large-signal load changes and nonlinear dynamic system models.

The first task is to accurately represent the large-signal jump behavior of practical loads. Methods of modeling stochastic load behavior without Gaussian process approximations have been proposed in the field of nonintrusive load monitoring (NILM). The objective of NILM is to obtain a detailed description of the behavior of devices in a system without monitoring each device individually [12], [13]. This is accomplished using probabilistic models of device behavior. A successful subset of NILM methods employs hidden Markov models (HMMs) to describe devices [14]–[17]. HMM-based load models transition through a discrete set of states, or modes, each corresponding to a stationary distribution of power consumption. Transitions between modes enable these models to represent the large-signal jump events characteristic of practical loads. An additional advantage of HMMs is that they can be trained to represent individual device behavior and then combined as needed to construct models of composite multidevice loads. This is particularly useful when modeling multiple devices at different locations in a distribution system. The methods for constructing and manipulating device models proposed in [17] are the basis for the load representation in this article.

The next task, which is much more technically challenging, is to predict the influence of stochastic behavior on system parameters. Previous research in this area has primarily fallen into two categories. The first category is essentially data-driven, using copious data to develop either a model of the stochastic behavior to use for reliability predictions [18] or to gain insight into the expected system behavior for deterministic design [19]. Evaluation is primarily performed with Monte Carlo simulations. For example, in [19], solar power data was analyzed in the frequency domain. After designing a (deterministic) filter, system behavior was evaluated with a combination of actual data and Monte Carlo methods. The other category uses polynomial chaos [20]–[22], a formalism that transforms stochastic processes with a set of orthogonal bases, analogous to a Fourier series expansion for periodic signals. Polynomial chaos is an excellent approach for component tolerance studies and has also been applied to input uncertainty. Most applications in the power electronics domain have focused on circuit-oriented models, rather than state-space-oriented models, and have not addressed discrete-event systems.

This article proposes a method of obtaining appropriate descriptions by modeling converter and load behavior as a stochastic hybrid system (SHS). The SHS framework is a powerful modeling tool that includes continuous dynamics, instantaneous events, and a variety of random effects [23]. The framework is challenging due to its sheer generality but offers powerful machinery for system analysis. In particular, it is possible to describe the evolution of moments of dynamic states as a system of ordinary differential equations (ODEs). In [24], a conventional power system was modeled as an SHS. A similar approach was employed in [25] to analyze the stability of ac microgrid systems. The procedure for applying the SHS framework here is heavily influenced by the methods in [24], though the treatment of load behavior is different.

This article extends [26] and applies the generic SHS framework to a Markov jump linear system (MJLS) that results from linearizing a nonlinear system around a set of operating points represented by the modes of a continuous-time Markov chain. Similar to [24], this SHS is used to determine the dynamics of the moments of the states and modes. A mathematical framework and accompanying algorithm are then derived to convert the dynamical equations into conventional state-space matrix representation. This is the primary contribution of the article.

The proposed modeling approach is applicable regardless of system structure or the topologies of its constituent converters. To demonstrate the functionality of the approach and verify its accuracy, the algorithm is applied to a seven-bus dc microgrid system containing five dual active bridge (DAB) converters and multiple loads. The stochastic, time-varying behavior of the system's loads are described by Markov chains. The SHS model is used to analyze the impact of the loads' collective random influence on system dynamics by computing low order moments of important dynamic state variables.

The second contribution is a method of assessing the probability of soft-switching for each of the converters in the seven-bus system. The method leverages the state variable moment calculations enabled by the proposed system modeling approach. These moments are used to determine the probability of operating in the zero voltage switching (ZVS) regime. The system-level modeling algorithms make it possible to calculate moments with high computational efficiency. As a result, the moment calculations are easily integrated into iterative optimization methods, where alternative approaches to characterizing expected system behavior (e.g., Monte Carlo simulation) would be too slow and cumbersome to use. To illustrate this, an optimization routine is constructed around the ZVS prediction method and used to improve soft-switching performance by varying controller gain parameters. The ZVS prediction and optimization procedure is

presented in the context of the 7-bus system and the DAB topology, but its true value is as an exemplary embodiment of the SHS model's applications to practical design challenges. The intent of this contribution is not to provide a method for improving ZVS in DAB-based dc microgrids, but rather to illustrate how SHS model outputs may be used to improve specific system and converter performance attributes.

The rest of this article is structured as follows. Section II reviews relevant aspects of the SHS framework. The conversion of the SHS model to state-space matrices is described in Section III. The algorithms described in Section III are then applied to a seven-bus system. The key elements of this system and their respective mathematical representations are discussed in Section IV. The seven-bus system and its dynamic model are introduced in Section IV-A. Section IV-B describes the load models and the process of incorporating their influence into the SHS model. The method of predicting the probability of ZVS is discussed in Section IV-C. The verification experiments are described in Section V, including the demonstration of soft-switching performance improvement as a gain-tuning optimization problem. Finally, Section VI concludes the article.

II. Background

The SHS framework is extremely general, and only a limited subset of its descriptive capability is used in this article. This section reviews the fundamentals of the SHS approach that are relevant to the proposed method. A more comprehensive review of SHS formalisms and their application to similar systems can be found in [23], [24], and [27].

Consider a dynamic model with the form

$$\dot{x} = f(x, y, u) \tag{1}$$

$$0 = g(x, y, u) \tag{2}$$

where x, y, and u are vectors denoting dynamic states, algebraic states, and inputs, respectively. For a given operating point, there is a corresponding affine model defined by

$$\dot{x} = Ax + Bu + C \tag{3}$$

$$y = Dx + Eu + F. \tag{4}$$

The affine terms C and F allow the use of the large-signal state x and output y, rather than small-signal perturbations.

Let $Q(t)$ be a homogenous continuous-time Markov chain (CTMC) that transitions between a set of discrete modes $\mathcal{S}$ according to a transition rate matrix Λ. At some time t, the occupation probabilities for each mode $s \in \mathcal{S}$ are denoted $\pi_s(t)$. Defining the occupation probability row vector $\pi = [\pi_1, \ldots, \pi_{|\mathcal{S}|}]$

$$\dot{\pi} = \pi\Lambda. \tag{5}$$

Each mode s corresponds to a set of inputs u_s. The SHS model consists of a family of affine models linearized at each u_s. The model is

$$\dot{X}(t) = A_s X(t) + B_s u_s + C_s \tag{6}$$

where $X(t)$ is a stochastic process that describes the continuous dynamic state. The transition rate matrix Λ fully determines mode transitions. That is, mode transitions are not explicitly time or state-dependent. A reset map defines how states and modes change on each transition. The reset map is denoted ϕ_{ij}, where $i, j \in \mathcal{S}$ are the modes before and after the transition, respectively. In this case, the function of the reset map is to avoid any discontinuities in the dynamic state. Therefore, ϕ_{ij} is defined as

$$\phi_{ij}(q, x) = (j, x). \tag{7}$$

This definition agrees with [24], including the extra input q (denoting the value of random variable Q) that is always equal to i when the reset map activates.

The SHS framework enables analysis of the behavior of probabilistic moments of the state $X(t)$ directly. Using the extended generator for the SHS, a set of ordinary differential equations may be found for the moments. The extended generator is

$$(L\psi)(q, x) = \frac{\partial}{\partial x}\psi(q, x) \cdot (A_q x + B_q u_q + C_q) + \sum_{i,j \in \mathcal{S}} \lambda_{ij} \left((\psi(\phi_{ij}(q, x)) - \psi(q, x)) \right) \tag{8}$$

where $\psi(q, x)$ is a suitably smooth test function, each λ_{ij} is an element of matrix Λ, and L represents a Lie derivative. For the generator form shown in (8), which assumes that inputs are constant between mode transitions, $\psi(q, x)$ must be bounded and continuously differentiable with respect to x. More stringent requirements apply when the inputs are assumed to be stochastic. If inputs contain white noise components, $\phi(q, x)$ must be twice continuously differentiable with respect to x [23].

The generator becomes useful in Dynkin's formula, which describes the evolution of the expected value of the test function in terms of the underlying random variables

$$\frac{d}{dt}\mathbb{E}\left[\psi(Q(t), X(t))\right] = \mathbb{E}\left[(L\psi)(Q(t), X(t))\right]. \tag{9}$$

To extract conditional moments of $X(t)$, the test function is defined as

$$\psi_i^{(m)}(q, x) = \delta_i(q) x^{(m)} \tag{10}$$

where $\delta_i(q)$ is the Kronecker delta function and m is a vector of moment orders [24]. For a system with N dynamic states, m is an N-element row vector and $x^{(m)}$ defined as

$$x^{(m)} = \prod_{k=1}^{N} x_k^{m_k}. \tag{11}$$

For a given mode i, the expected value of $\psi(q, x)$ is equal to the conditional moments of $X(t)$

$$\mathbb{E}\left[\psi_i^{(m)}(q, x)\right] = \mathbb{E}\left[X^{(m)}(t) \middle| Q(t) = i\right] \pi_i(t). \tag{12}$$

The unconditional moments of $X(t)$ may then be computed by the law of total expectation

$$\mathbb{E}\left[X^{(m)}(t)\right] = \sum_{i \in \mathcal{S}} \mathbb{E}\left[\psi_i^{(m)}(q, x)\right]. \tag{13}$$

Therefore, the evolution of the dynamic state moments is described by the set of ODEs corresponding to time derivatives of

$\mathbb{E}[\psi_i^{(m)}(q,x)]$. To simplify notation, let the conditional moments be denoted by

$$\mu_i^{(m)}(t) = \mathbb{E}\left[\psi_i^{(m)}(q,x)\right]. \tag{14}$$

Then according to (9), the ODEs of interest are

$$\dot{\mu}_i^{(m)}(t) = \mathbb{E}\left[(L\psi_i^{(m)})(Q(t),X(t))\right]. \tag{15}$$

Conditional moments of algebraic states may be computed from the conditional moments of $X(t)$. Let conditional moments of the process $Y(t)$ be denoted $\zeta^{(m)}(t)$. Then the conditional moments are

$$\zeta_i^{(m)}(t) = \mathbb{E}\left[(D_iX(t)+E_iu_i+F_i)^{(m)}\middle|Q(t)=i\right]\pi_i(t). \tag{16}$$

Much of the practical difficulty in applying the SHS framework lies in computing usable expressions for the right-hand sides of (15) and (16). An expression for the right-hand side of (15) is given below, slightly modified from the form given in [24]

$$\dot{\mu}_i^{(m)}(t) = \sum_{p=1}^{N} m_p\left(\sum_{r=1}^{N} a_{pr}^{(i)}\mu_i^{(m-e_p+e_r)}(t) + \mu_i^{(m-e_p)}(t)v_{i,p}\right) + \sum_{j\in\mathcal{S}_i^-}\lambda_{ji}\mu_j^{(m)}(t) - \sum_{k\in\mathcal{S}_i^+}\lambda_{ik}\mu_i^{(m)}(t). \tag{17}$$

In this equation, $a_{pr}^{(i)}$ is the pth row, rth column element of A_i, $v_{i,p}$ is the pth element of vector $v_i = B_iu_i + C_i$, and $\mathcal{S}_i^-$ and $\mathcal{S}_i^+$ denote the sets of modes that transition into and out of mode i, respectively. Vectors e_p and e_r are elementary row vectors, that is, row vectors of all zeros except that the pth or rth element is 1.

III. SHS Microgrid Model

A. Matrix Formulation of SHS Model

Let $\mu_i^{|n|}(t)$ denote the set of all nth moments of $X(t)$ conditional on mode i. That is, $\mu_i^{|n|}(t)$ is a column vector of all moments $\mu_i^{(m)}$, as defined in (14), for which $\|m\|_1 = n$. For proper ordering with respect to the states

$$\mu_i^{|n|}(t) = \mathbb{E}\left[X^{\otimes n}(t)|Q(t)=i\right]\pi_i(t) \tag{18}$$

where $\otimes$ is the Kronecker product and $X^{\otimes n}$ is a Kronecker power, that is, $X\otimes X\cdots\otimes X$ with n factors. By convention, $X^{\otimes 0}=1$. In this way, the 0th order moments are the mode occupation probabilities

$$\mu_i^{|0|}(t) = \mathbb{E}\left[1\middle|Q(t)=i\right]\pi_i(t) = \pi_i(t). \tag{19}$$

First and second order moments are

$$\mu_i^{|1|}(t) = \mathbb{E}\left[X(t)\middle|Q(t)=i\right]\pi_i(t) \tag{20}$$

$$\mu_i^{|2|}(t) = \mathbb{E}\left[X(t)\otimes X(t)\middle|Q(t)=i\right]\pi_i(t). \tag{21}$$

Similarly for higher-order moments if needed. To represent moments for all modes, let vector $\mu^{|n|}(t)$ be defined as

$$\mu^{|n|}(t) = \begin{bmatrix}\mu_1^{|n|}(t)\\ \vdots \\ \mu_M^{|n|}(t)\end{bmatrix}. \tag{22}$$

In this way, $\mu^{|0|}(t)\in\mathbb{R}^{M\times 1}$ contains mode occupation probabilities ($\mu^{|0|}=\pi^T$), $\mu^{|1|}(t)\in\tilde{}\mathbb{R}^{NM\times 1}$ contains all first order moments, $\mu^{|2|}(t)\in\tilde{}\mathbb{R}^{N^2M\times 1}$, contains all second order moments, and so on.

With this construction, many redundant terms are included. For a system with N dynamic states, the number of unique nth order moments is

$$N_u(n) = \binom{N+n-1}{n}. \tag{23}$$

Consider two elements of $X(t)$, X_k and X_ℓ, $k,\ell\in\{1,\ldots,N\}$, which are both scalars. As constructed, $\mu^{|2|}$ will include both $\mathbb{E}[X_k(t)X_\ell(t)]$ and $\mathbb{E}[X_\ell(t)X_k(t)]$. These scalar products are actually identical, and so must be eliminated. However, the construction process is straightforward, as is the set of matrix operations needed to eliminate redundancies. The vectors of unique moments are denoted $\hat{\mu}_i^{|n|}(t)$. In this article, this difference in notation is only necessary for the second order moments, since $\hat{\mu}_i^{|n|}(t) = \mu_i^{|n|}(t)$ for $n<2$.

For the SHS formulation used in this article, moment dynamic equations depend only on moments of equal or lower order, avoiding the need for moment-closure methods [24]. In fact, the dynamics of moments of order n are only directly dependent on moments of order n and $n-1$, as is clear from (17). For a given moment characterized by m, $\dot{\mu}_i^{(m)}(t)$ depends on $\mu_i^{(m-e_p+e_r)}(t)$, $\mu_i^{(m-e_p)}(t)$, $\mu_i^{(m)}(t)$, and $\mu_j^{(m)}(t)$ for other modes $j\in\mathcal{S}$. Recall that the order of moment $\mu_i^{(m)}(t)$ is equal to the one-norm of m. Trivially, $\mu_i^{(m)}(t)$ and $\mu_j^{(m)}(t)$ have the same order. If the order of $\mu_i^{(m)}(t)$ is n, then since e_p and e_r are unit vectors, the orders of $\mu_i^{(m-e_p+e_r)}(t)$ and $\mu_i^{(m-e_p)}(t)$ must be n and $n-1$, respectively.

Consequently, it is possible to express the system of ODEs for nth order moments as

$$\dot{\mu}^{|n|}(t) = G^{(n)}\mu^{|n|}(t) + H^{(n)}\mu^{|n-1|}(t). \tag{24}$$

Matrices $G^{(n)}$ and $H^{(n)}$ follow from (17), but provide a more manageable structure to the definition of the SHS model.

Simplified expressions for $G^{(n)}$ and $H^{(n)}$ are given here for low-order moments. The 0th order moments are the mode occupation probabilities of the CTMC. Therefore $G^{(0)}=\Lambda^T$ and $H^{(0)}=0$, where the transpose is due to the fact $\mu^{|0|}(t)$ is a column vector. For the first and second order moments, both $G^{(n)}$ and $H^{(n)}$ may be constructed primarily as block diagonal

combinations of submatrices for each mode

$$G^{(n)} = \begin{bmatrix} G_1^{(n)} & 0 & \cdots & 0 \\ 0 & G_2^{(n)} & \cdots & 0 \\ \vdots & \vdots & \ddots & \vdots \\ 0 & 0 & \cdots & G_M^{(n)} \end{bmatrix} + \left(\Lambda^T \otimes I(N^n)\right) \quad (25)$$

$$H^{(n)} = \begin{bmatrix} H_1^{(n)} & 0 & \cdots & 0 \\ 0 & H_2^{(n)} & \cdots & 0 \\ \vdots & \vdots & \ddots & \vdots \\ 0 & 0 & \cdots & H_M^{(n)}, \end{bmatrix} \quad (26)$$

where $I(N^n)$ is the N^n-dimensional identity matrix. In the case of first order moments, the submatrices for each mode are

$$G_i^{(1)} = A_i \quad (27)$$

$$H_i^{(1)} = v_i. \quad (28)$$

For second-order moments, the submatrices are calculated using a transformation matrix, W_m, which is constant for all modes

$$G_i^{(2)} = W_m \left(I(N) \otimes A_i\right) \quad (29)$$

$$H_i^{(2)} = W_m \left(I(N) \otimes v_i\right). \quad (30)$$

The role of W_m is to describe the structure of the moments. Each row of W_m corresponds to the dynamic equation for a particular conditional second order moment. The elements of W_m correspond to the values of the coefficient m_p in (17). Since W_m describes second order moments, all rows and columns sum to 2. Note that a transformation appears in the equations for second order moments, but not in equations for first-order moments, i.e., (27) and (28). The same connection to values of m_p in (17) applies to these equations, but if a transformation was defined it would simply be the identity matrix.

The sparsity pattern of W_m for a simple system with $N = 3$ states is shown in Fig. 1. To illustrate how W_m corresponds to moment relationships, conditional second order moments are shown on the horizontal and vertical axes. For legibility, time dependence and conditioning are omitted from the notation used in the figure.

Matrix W_m represents relationships between second-order moments. Since moments $\mathbb{E}[X_1(t)X_2(t)|Q(t) = q]$ and $\mathbb{E}[X_2(t)X_1(t)|Q(t) = q]$ are the same, the equations that govern their dynamics must both depend on exactly the same two moments. Furthermore, moments whose dynamics depend on $\mathbb{E}[X_1(t)X_2(t)|Q(t) = q]$ must also depend on $\mathbb{E}[X_2(t)X_1(t)|Q(t) = q]$. Fig. 1 shows that this is the case.

A convenient way to decompose the structure of W_m is to separate each moment's dependencies into self-dependence and dependence on its equivalent moment. This separation may be accomplished as

$$W_m = I(N^2) + W_s + W_c \quad (31)$$

where the identity matrix describes each moment's self-dependence, W_s adds another self-dependence for moments

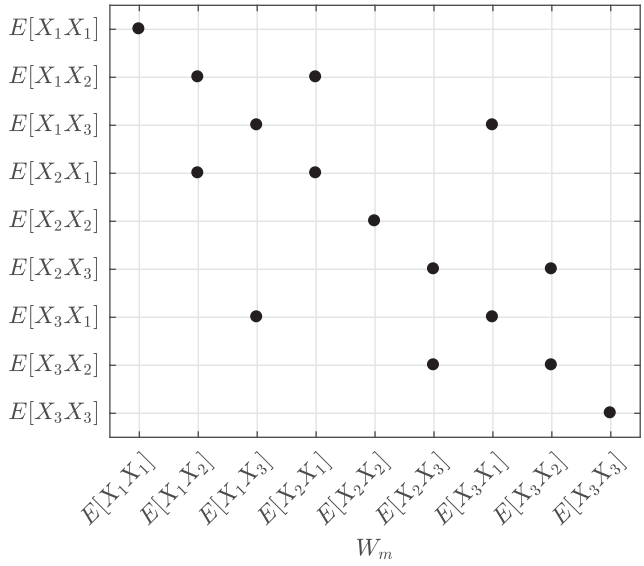

Fig. 1. Example of transformation matrix W_m for a 3-state system.

of the form $\mathbb{E}[X_i(t)X_i(t)|Q(t) = q]$, and W_c describes dependence on the equivalent moment (that is, the equivalence of $\mathbb{E}[X_i(t)X_j(t)|Q(t) = q]$ and $\mathbb{E}[X_j(t)X_i(t)|Q(t) = q]$ for $i \neq j$). The decomposition is shown graphically in Fig. 2. The nonzero elements W_s and W_c are

$$W_s\big(N(i-1)+i, N(i-1)+i\big) = 1, \quad \forall i \in \{1, \ldots, N\} \quad (32)$$

$$W_c\big(N(i-1)+j, N(j-1)+i\big) = 1, \quad \forall i, j \in \{1, \ldots, N\}, \quad i \neq j. \quad (33)$$

B. Elimination of Redundant Second Order Moments

The equivalent moments contained in $\mu_i^{|2|}(t)$ decrease the computational efficiency of the SHS model. Moreover, matrix $G_i^{(2)}$ will be rank-deficient unless redundant moments are eliminated, meaning stationary moment solutions cannot be calculated through linear equations. However, redundant moments may be eliminated from the system using the transformation matrix W_m and its decomposed forms W_c and W_s. Redundant moments are eliminated at the submatrix level, such that the reduced system is constructed through the same block-diagonal procedure. Considering only unique second order moments, the reduced system is

$$\dot{\hat{\mu}}^{|2|}(t) = \hat{G}^{(2)}\hat{\mu}^{|2|}(t) + \hat{H}^{(2)}\mu^{|1|}(t) \quad (34)$$

$$\hat{G}^{(2)} = \begin{bmatrix} \hat{G}_1^{(2)} & 0 & \cdots & 0 \\ 0 & \hat{G}_2^{(2)} & \cdots & 0 \\ \vdots & \vdots & \ddots & \vdots \\ 0 & 0 & \cdots & \hat{G}_M^{(2)} \end{bmatrix} + \left(\Lambda^T \otimes I(N_u(2))\right) \quad (35)$$

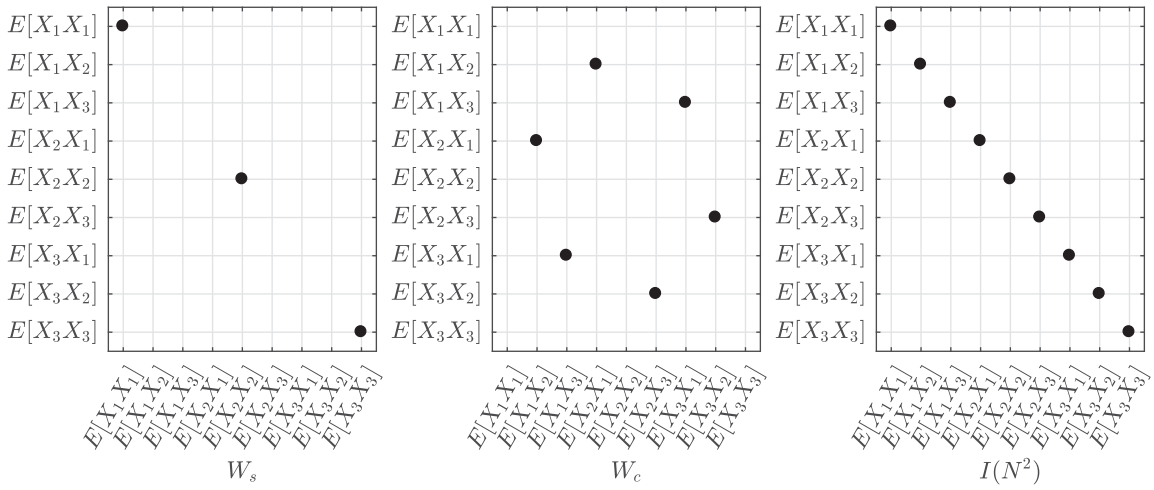

Fig. 2. Decomposition of W_m into W_s, W_c, and $I(N^2)$ for a three-state system.

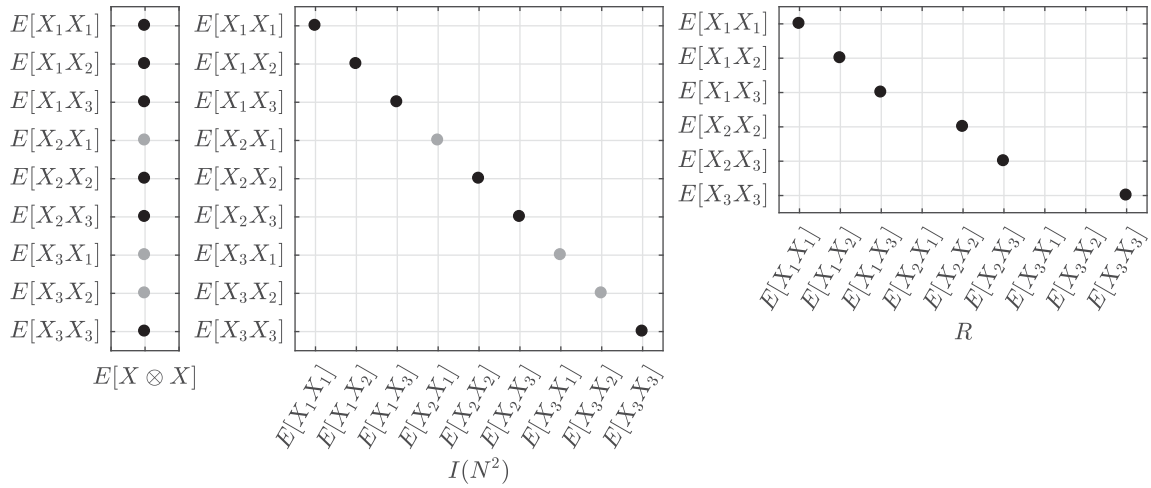

Fig. 3. Specification of R from indices of unique moments.

$$\hat{H}^{(2)} = \begin{bmatrix} \hat{H}_1^{(2)} & 0 & \cdots & 0 \\ 0 & \hat{H}_2^{(2)} & \cdots & 0 \\ \vdots & \vdots & \ddots & \vdots \\ 0 & 0 & \cdots & \hat{H}_M^{(2)} \end{bmatrix}. \tag{36}$$

The process of eliminating redundant moments consists of two linear transformations. First, rows of $G_i^{(2)}$ that describe dynamics of redundant moments must be eliminated. Second, columns of $G_i^{(2)}$ corresponding to dependence on equivalent moments must be summed together. One additional matrix, denoted R, describes these transformations. Let $\hat{\mu}_i^{|2|}(t) = R\mu_i^{|2|}(t)$, where R eliminates all redundant moments from $\mu_i^{|2|}(t)$. Matrix R is easily specified from the locations of unique moments in $\mu_i^{|2|}(t)$. The indices of the unique moments are an ordered set of $N_u(2)$ integers, defined by

$$S_u = \bigcup_{i=1}^{N} \{(i-1)N + i, \ldots, iN\}. \tag{37}$$

Then, the $N_u(2)$ rows of R are the rows of the N^2 identity matrix that correspond to unique moments: if j is the ith element of S_u, the ith row of R is the jth row of $I(N^2)$.

In the case of the simplified three-moment system, the indices of unique moments are

$$S_u = \{1, 2, 3\} \cup \{5, 6\} \cup \{7\}. \tag{38}$$

For this system, the fourth element of S_u is 5. Therefore, the fourth row, fifth column element of R is equal to 1. This is shown graphically in Fig. 3.

Matrix R is exactly the transformation needed to eliminate redundant moment equations from the model. Premultiplying $G_i^{(2)}$ and $H_i^{(2)}$ by R eliminates rows that describe dynamics of redundant moments. This is all that is needed to determine $\hat{H}_i^{(2)}$ from $H_i^{(2)}$. To complete the definition of $\hat{G}_i^{(2)}$, columns of $G_i^{(2)}$ that correspond to dependence on equivalent moments must be summed. Relationships between equivalent moments are contained in W_m. The relevant information is in W_c and $I(N^2)$; the additional self-dependence described by W_s is irrelevant to moment equivalence. Postmultiplying $G_i^{(2)}$ by $(W_c + I(N^2))^T$

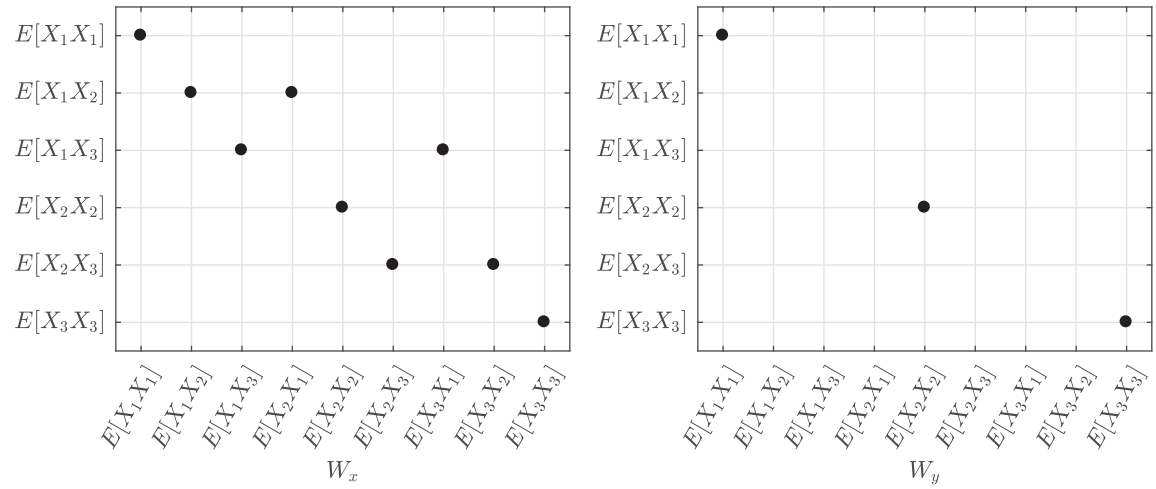

Fig. 4. Sparsity pattern of final transformation matrices used to calculate reduced subsystem matrices.

sums the necessary columns. The full transformation is

$$\hat{G}_i^{(2)} = RG_i^{(2)}\left[R(W_c + I(N^2))\right]^T \tag{39}$$

$$\hat{H}_i^{(2)} = RH_i^{(2)}. \tag{40}$$

In comparison to the submatrices in (29) and (30), these definitions produce a second order system with significantly reduced size. More importantly, matrix $\hat{G}^{(2)}$ will always have full rank, making it possible to solve for stationary moments.

C. Efficient Algorithm to Determine Second-Order Moment Dynamics

A more efficient alternative to (39) and (40) is to directly calculate $\hat{G}_i^{(2)}$ and $\hat{H}_i^{(2)}$, rather than reducing them from $G_i^{(2)}$ and $H_i^{(2)}$. Define two new transformations, W_x and W_y, as

$$W_x = R\big(W_c + I(N^2)\big) \tag{41}$$

$$W_y = RW_s. \tag{42}$$

Sparsity patterns for these matrices are shown in Fig. 4. Combining (29) and (30), and the various transformation matrices, the reduced subsystem matrices may be calculated directly from W_x, W_y, A_i, and v_i as

$$\hat{G}_i^{(2)} = (W_x + W_y)\left(I(N) \otimes A_i\right)\left(W_x^T\right) \tag{43}$$

$$\hat{H}_i^{(2)} = (W_x + W_y)\left(I(N) \otimes v_i\right). \tag{44}$$

The definitions in (41) and (42) are only given for clarity of derivation. In practice, W_x and W_y are more efficiently constructed with the simple algorithm in Fig. 5. Both are highly sparse, so direct construction is more efficient than multiplication. W_x and W_y are the only transformations required to calculate the reduced subsystem matrices, so the ability to specify them directly is a significant advantage. After W_x and W_y have been constructed according to the pseudocode in Fig. 5, the final SHS model may be formed from (43) and (44) without calculating R, W_m, W_s, or W_c.

```
W_x ← [0]_{N_u(2),N^2}, W_y ← [0]_{N_u(2),N^2}
k ← 1
for i ← 1, ··· , N do
    W_y(k, N(i − 1) + i) ← 1
    for j ← i, ··· , N do
        W_x(k, N(i − 1) + j) ← 1
        W_x(k, N(j − 1) + i) ← 1
        k ← k + 1
    end for
end for
```

Fig. 5. Pseudocode for construction of W_x and W_y.

D. Final Model and Steady-State Moments

After reducing the second order system, the final model for low order moments is

$$\dot{\mu}^{|0|}(t) = G^{(0)}\mu^{|0|}(t) \tag{45}$$

$$\dot{\mu}^{|1|}(t) = G^{(1)}\mu^{|1|}(t) + H^{(1)}\mu^{|0|}(t) \tag{46}$$

$$\dot{\hat{\mu}}^{|2|}(t) = \hat{G}^{(2)}\hat{\mu}^{|2|}(t) + \hat{H}^{(2)}\mu^{|1|}(t) \tag{47}$$

where $G^{(0)} = \Lambda^T$ and $G^{(1)}$, $H^{(1)}$, $\hat{G}^{(2)}$, and $\hat{H}^{(2)}$ are specified by submatrices in (27), (28), (43), and (44), respectively. Noting that $\hat{\mu}^{|n|}(t) = \hat{\mu}^{|n|}(t)$, $\hat{G}^{(n)} = G^{(n)}$, and $\hat{H}^{(n)} = H^{(n)}$ for $n = 0$ and $n = 1$, the general form of an nth order SHS model may be expressed as

$$\dot{\hat{\mu}}^{|n|}(t) = \hat{G}^{(n)}\hat{\mu}^{|n|}(t) + \hat{H}^{(n)}\hat{\mu}^{|n-1|}(t) \tag{48}$$

$$\hat{G}^{(n)} = \begin{bmatrix} \hat{G}_1^{(n)} & 0 & \cdots & 0 \\ 0 & \hat{G}_2^{(n)} & \cdots & 0 \\ \vdots & \vdots & \ddots & \vdots \\ 0 & 0 & \cdots & \hat{G}_M^{(n)} \end{bmatrix} + \left(\Lambda^T \otimes I(N_u(n))\right) \tag{49}$$

$$\hat{H}^{(n)} = \begin{bmatrix} \hat{H}_1^{(n)} & 0 & \cdots & 0 \\ 0 & \hat{H}_2^{(n)} & \cdots & 0 \\ \vdots & \vdots & \ddots & \vdots \\ 0 & 0 & \cdots & \hat{H}_M^{(n)} \end{bmatrix}. \quad (50)$$

Submatrices $\hat{G}_i^{(n)}$ and $\hat{H}_i^{(n)}$ are

$$\hat{G}_i^{(n)} = R^{(n)} W_m^{(n)} \left(I(N^{n-1}) \otimes A_i \right) \left[R^{(n)} \left(W_c^{(n)} + I(N^n) \right) \right] \quad (51)$$

$$\hat{H}_i^{(n)} = R^{(n)} W_m^{(n)} \left(I(N^{n-1}) \otimes v_i \right) \left[R^{(n-1)} \left(W_c^{(n-1)} + I(N^{n-1}) \right) \right] \quad (52)$$

where $R^{(n)}$, $W_m^{(n)}$, and $W_c^{(n)}$ are transformation matrices for the *n*th order moments.

This system is suitable for predicting moment dynamics. In some cases, however, it may be desirable to simply compute the moments for steady-state behavior. Let t_F represent some final time at which the stationary distribution has been reached, and the left-hand side of (48) is 0. The zeroth moments are the stationary distribution of the CTMC, or $\pi(t_F)$. Therefore, $\mu^{|0|}(t_F)$ may be determined by solving $0 = \Lambda^T \mu^{|0|}(t_F)$ with the constraint

$$\sum_{i=1}^{M} \mu_i^{|0|}(t_F) = 1. \quad (53)$$

The rest of the stationary moments are then

$$\hat{\mu}^{|n|}(t_F) = \left(\hat{G}^{(n)} \right)^{-1} \left(-\hat{H}^{(1)} \hat{\mu}^{|n-1|}(t_F) \right). \quad (54)$$

IV. Application to DC Microgrids Based on DAB Converters

A. Dynamic DC Microgrid Model

The general SHS framework described in Section III is usable for a wide range of systems, as long as the switched affine model given in (3) to (7) is appropriately accurate. In this article, the target application is a dc microgrid, which in general consists of dc–dc converters, sources, lines, and loads.

While the SHS model construction algorithm described in Section III is applicable to a diverse range of systems, it is necessary to select a specific system for the purposes of demonstration and validation. The SHS models are built on top of deterministic dynamic models, which are specific to the systems under consideration. A full derivation of the deterministic dynamic model of the system used for validation experiments is neither necessary nor particularly valuable to the development of the proposed modeling method. However, detailed knowledge of this model is essential for reproducing the results of verification experiments. To manage scope without sacrificing reproducibility, the seven-bus system shown in Fig. 6 is chosen as the system under consideration. A detailed model of this exact system was derived in [28].

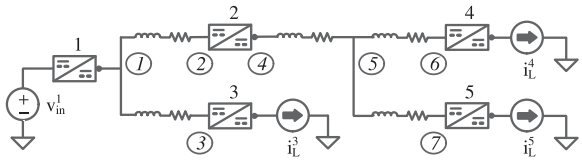

Fig. 6. A seven-bus test system.

In addition to detailing the specific model under consideration in this article, reference [28] also describes a general an approach to constructing system-level dynamic models of multiconverter systems. The process is similar to how large power system models are created from individual synchronous generator models and impedance networks. The focus of [28] is combining averaged models of DAB converters, but the methods apply equally to other dc–dc converter topologies as well. A similar approach is described in [29] for multiconverter systems with specific treatment of inverters and buck, boost, and buck-boost dc–dc converters.

B. Load Models and System Inputs

The deterministic dynamic model of the microgrid system has the standard form shown in (1) and (2). For the system shown in Fig. 6, the input vector u includes the source voltage v_{in}^1, load currents i_L^3, i_L^4, and i_L^5, and voltage reference setpoints for each of the converters in the system. These inputs are time-varying, and all are potential sources of uncertainty. That is, each input could be a stochastic process. For the purposes of this article, both the source voltage and the voltage references are constant, and only the load currents behave randomly. To use the methods described in Section III, the combined behavior of the loads must be described by a CTMC and the nonlinear system model must be converted into a switched affine model. Each mode of the CTMC corresponds to one possible permutation of load current inputs. The affine model is generated by linearizing the system around the steady-state response to load current values for each mode of the CTMC. The CTMC is constructed from individual models of load devices.

Individual load models are discrete-time Markov chains. The DTMC for a load device may either be specified directly based on expert knowledge of the device's behavior or, more commonly, created from empirical measurements. This process is referred to as "training" the model. Load device models may be visualized as finite state machines, where each state corresponds to a different value of current draw. This is shown in Fig. 7 for the seven-bus system. An individual converter may serve multiple load devices. For instance, in Fig. 7, the load for DAB 3 consists of two devices. The device on the left has three states; the device on the right has two states.

The DTMC for each individual load i is defined by a set of modes of size M_i, mode transition probability matrix $P_i \in \mathbb{R}^{M_i \times M_i}$, possible output values $I_{Li} \in \mathbb{R}^{1 \times M_i}$, and a sample rate T_S. At each sample time, the probability of the ith device transitioning from mode j to mode k is element $p_{i,jk}$ of P_i. Each mode j corresponds to a single value of load current $I_{Li,j}$.

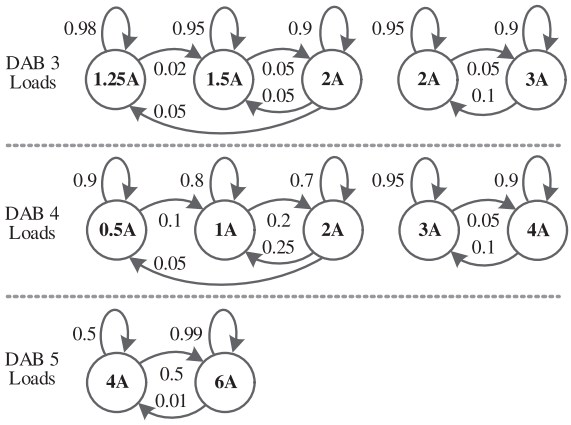

Fig. 7. Markov chains for loads in 7-bus system experiments.

The DTMC is trained using maximum likelihood estimation according to the procedure described in [17].

To model the complete system, a single, unified DTMC that represents all of the loads is needed. The complete system will have a set of modes M, transition matrix P, and load currents I_L (without a device-specific subscript). The composite model is constructed recursively. When one load is included, $M = M_1$, $P = P_1$, and $I_L = I_{L1}$. To add each subsequent device, set

$$P \leftarrow P_i \otimes P \tag{55}$$

$$I_L \leftarrow I_{Li} \otimes \mathbf{1}(M) + \mathbf{1}(M_i) \otimes I_L \tag{56}$$

$$M \leftarrow MM_i \tag{57}$$

where $\mathbf{1}(M)$ is a column vector of M elements all equal to 1. This process is a slight modification of the process described in [17].

For the case of a single load, each mode corresponds to a scalar value of current (that is, mode j corresponds to $I_{L,j}$). For the general case, each mode corresponds to a vector of load currents. For example, the seven-bus system shown in Fig. 6 has three load buses, so each mode corresponds to a 1×3 vector. A given load will typically connect to only one load bus, so only one element of the row vector will be nonzero. If load i has two modes, then $I_{Li} \in \mathbb{R}^{2\times 3}$. The combination process increases the number of rows of I_L but not the number of columns, so that for the combined five loads illustrated in Fig. 7, $I_L \in \mathbb{R}^{72\times 3}$.

After executing (55)–(57) for all of the loads, the composite model will describe a DTMC with M modes and transition probability matrix P. In general, a DTMC may not be directly converted to a CTMC. However, knowing that the DTMC was created from uniformly sampled continuous-time signals, and assuming that the sample rate was sufficiently high, the CTMC may be approximated. With a sample period of T_s, the transition rate matrix Λ has elements

$$\lambda_{ii} = -\frac{1 - p_{ii}}{T_s} \tag{58}$$

$$\lambda_{ij} = \frac{p_{ij}}{T_s}, \quad i \neq j. \tag{59}$$

The CTMC with state $Q(t)$ is governed by Λ and has M modes, each corresponding to a load current vector $I_L(Q, :)$. These modes, and their corresponding load current vectors, provide the information necessary to construct the switched affine model of the microgrid system.

C. Prediction of ZVS Performance

The methods in Section III do not depend on the deterministic system or converter models. However, the ZVS prediction and improvement example does require some basic description of an individual DAB converter model.

The DAB converters in the system under consideration are internally deterministic and modeled according to the procedure in [30]. The converters are voltage-controlled and serve either current source loads or other downstream converters. Single-phase-shift (SPS) modulation is used, the simplest form, in which all four legs of the DAB switch at 50% duty ratio, the two legs of each bridge are 180° out of phase, and the phase shift between the two bridges is used for control (translated into an effective duty ratio d). A simple PI controller on the voltage is used to determine d according to

$$\dot{\gamma} = k_i(v_{ref} - v_o) \tag{60}$$

$$d = k_p(v_{ref} - v_o) + \gamma \tag{61}$$

where k_p and k_i are the gains, v_{ref} is an exogenous reference, and v_o is the actual output voltage. The conditions for ZVS may be expressed in terms of phase shift and voltage gain [31]–[33]. Assuming forward power transfer, ZVS occurs in both H-bridges when the following inequalities are satisfied:

$$d \geq \frac{1}{2} - \frac{v_o}{2v_c} \tag{62}$$

$$d \geq \frac{1}{2} - \frac{v_c}{2v_o} \tag{63}$$

where v_c is the input voltage, referred across the transformer. Since both v_o and v_c are strictly positive, these inequalities may be rearranged as

$$2dv_c + v_o - v_c \geq 0 \tag{64}$$

$$2dv_o + v_c - v_o \geq 0. \tag{65}$$

Further, since d is a function of the controller states, these conditions may be expressed entirely in terms of the states and inputs of the DAB model. The resulting expressions are denoted as $h_d(x, u)$ and $h_u(x, u)$, with subscripts indicating that they pertain to the conditions for voltage step-down and step-up operation, respectively

$$h_d(x, u) \triangleq 2v_c\left(k_p(v_{ref} - v_o) + \gamma\right) + v_o - v_c \tag{66}$$

$$h_u(x, u) \triangleq 2v_o\left(k_p(v_{ref} - v_o) + \gamma\right) + v_c - v_o. \tag{67}$$

In the context of the deterministic model, ZVS operation in a given converter may be determined by checking whether $h_d(x, u) \geq 0$ and $h_u(x, u) \geq 0$.

The SHS framework may be used to determine the uncentered moments of all of the discrete and continuous states, as well as algebraic functions of the states. The moments may be used

to evaluate operating conditions, including the probability of satisfying certain requirements like ZVS, that are expressed as an algebraic function $h(x,u)$. For simplicity, a scalar-valued function is considered here.

For a given mode Q, the input is u_q and the corresponding steady-state operating point is x_q. Near this equilibrium

$$h(x,u) \approx D_q x + E_q u_q + f_q \tag{68}$$

where D_q and E_q are derivative vectors and f_q is a constant scalar offset

$$D_q = \left.\frac{\partial h(x,u)}{\partial x}\right|_{\substack{x=x_q \\ u=u_q}} \tag{69}$$

$$E_q = \left.\frac{\partial h(x,u)}{\partial u}\right|_{\substack{x=x_q \\ u=u_q}} \tag{70}$$

$$f_q = h(x_q,u_q) - D_q x_q - E_q u_q. \tag{71}$$

The conditional moments given by (16) may be simplified for the scalar case. Defining $\xi_i^{(n)}$ to be the conditional moments of $h(x,u)$ in mode i

$$\xi_i^{(n)}(t) = r_i^n \mu_i^{|0|}(t) + \sum_{k=1}^{n} \binom{n}{k} r_i^{n-k} D_i^{\otimes k} \mu_i^{|n|}(t) \tag{72}$$

where again $D_i^{\otimes k}$ is the kth Kronecker power and r_i is defined as

$$r_i = E_i u_i + f_i. \tag{73}$$

The first few moments of $\xi_i^{(n)}(t)$ are

$$\xi_i^{(1)}(t) = r_i \mu_i^{|0|}(t) + D_i \mu_i^{|1|}(t) \tag{74}$$

$$\xi_i^{(2)}(t) = r_i^2 \mu_i^{|0|}(t) + 2 r_i D_i \mu_i^{|1|}(t) + (D_i \otimes D_i)\, \mu_i^{|2|}(t). \tag{75}$$

The second order moment can alternatively be expressed as a function of unique second order dynamic state moments using the transformation (41)

$$\xi_i^{(2)}(t) = r_i^2 \mu_i^{|0|}(t) + 2 r_i D_i \mu_i^{|1|}(t) + (D_i \otimes D_i)\left(W_x^T\right) \hat{\mu}_i^{|2|}(t). \tag{76}$$

Finally, the unconditional moments are the sum of each the conditional moments for each mode

$$\mathbb{E}\left[h(x,u)^n\right] = \xi^{(n)}(t) = \sum_{i=1}^{M} \xi_i^{(n)}(t). \tag{77}$$

Using the Cantelli inequality, bounds on the probability of a condition on $h(x,u)$ can be defined in terms of first and second moments. For generic random variable X and constant a, the Cantelli inequality is [34]

$$\mathbb{P}\left[(X-\mu_X) \geq a\right] \begin{cases} \leq & \frac{\sigma_X^2}{\sigma_X^2 + a^2} \quad a \geq 0 \\ \geq & 1 - \frac{\sigma_X^2}{\sigma_X^2 + a^2} \quad a < 0 \end{cases} \tag{78}$$

TABLE I
CONTROL AND HARDWARE PARAMETERS FOR 7-BUS SYSTEM

Parameter	Value	Parameter	Value
C_{in}^1, C_{in}^2, C_{in}^3, C_o^1, C_o^2, C_o^3	200 μF	v_{ref}^1	48 V
C_{in}^4, C_{in}^5, C_o^4, C_o^5	40 μF	v_{ref}^2, v_{ref}^3	42 V
L_t^1, L_t^2, L_t^3, L_t^4, L_t^5	4 μH	v_{ref}^4, v_{ref}^5	36 V
f_s^1	40 kHz	k_p^1 / k_i^1	0.01 / 15
f_s^2	60 kHz	k_p^2 / k_i^2	0.01 / 10
f_s^3	75 kHz	k_p^3 / k_i^3	0.01 / 25
f_s^4	100 kHz	k_p^4 / k_i^4	0.001 / 25
f_s^5	90 kHz	k_p^5 / k_i^5	0.005 / 25

where μ_X and σ_X^2 are, respectively, the first and second central moments of X. Letting $a = -\mu_X$ the inequality is

$$\mathbb{P}\left[X \geq 0\right] \begin{cases} \leq & \frac{\sigma_X^2}{\sigma_X^2 + \mu_X^2} \quad \mu_X < 0 \\ \geq & 1 - \frac{\sigma_X^2}{\sigma_X^2 + \mu_X^2} \; \mu_X \geq 0. \end{cases} \tag{79}$$

Applying this inequality to $h(x,u)$, and substituting raw uncentered moments for central moments, the upper limits and lower limits on the probability $\mathbb{P}[h(x,u) \geq 0]$ are

$$\mathbb{P}\left[h(x,u) \geq 0\right] \geq \begin{cases} \frac{(\xi^{(1)}(t))^2}{\xi^{(2)}(t)}, & \xi^{(1)}(t) \geq 0 \\ 0, & \xi^{(1)}(t) < 0 \end{cases} \tag{80}$$

$$\mathbb{P}\left[h(x,u) \geq 0\right] \leq \begin{cases} 1, & \xi^{(1)}(t) \geq 0 \\ 1 - \frac{(\xi^{(1)}(t))^2}{\xi^{(2)}(t)}, & \xi^{(1)}(t) < 0. \end{cases} \tag{81}$$

These expressions are valid for $h_d(x,u)$, $h_u(x,u)$, and for any other functions that encode operating conditions as scalar comparisons to zero. Thus, ZVS probability may be determined from (80) and (81).

V. VERIFICATION

The verification experiments for this article consider a seven-bus test system. The system contains 5 DAB converters and is structured as shown in Fig. 6. All DAB converters are closed-loop, voltage-controlled. Inputs to the system-level model are source voltages/currents, load currents, and voltage reference commands for voltage controllers. The converter output terminals are indicated with a dot in Fig. 6. Hardware and control parameters are given in Table I. Randomness is introduced through the loads of converters 3, 4, and 5. Markov chains that describe the individual devices in these three loads are shown in Fig. 7.

Performance is assessed through comparisons of Monte Carlo simulations to predictions from the SHS model. The Monte Carlo analysis consists of 1000 independent simulations of a period of 15 ms. In all cases, the load devices begin mode 1 at $t = 0$ s, corresponding to the leftmost modes of the Markov chains shown in Fig. 7. The system experiences a transient response as the mode occupation probabilities approach the stationary distribution of the CTMC. The simulations use a discrete sample time of 1 μs. Unless otherwise specified, Monte

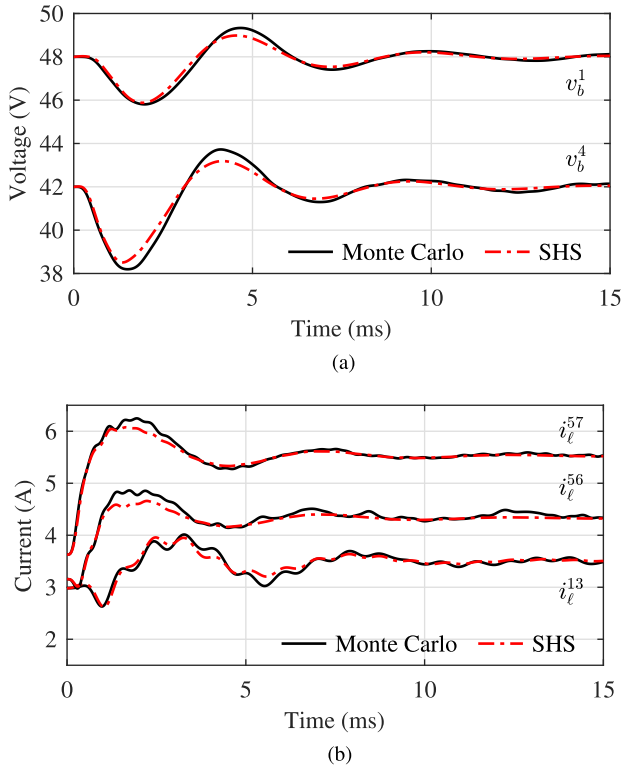

Fig. 8. Comparison of first moment dynamics obtained from Monte Carlo simulations to SHS model predictions. (a) Bus voltage first moments. (b) Line current first moments.

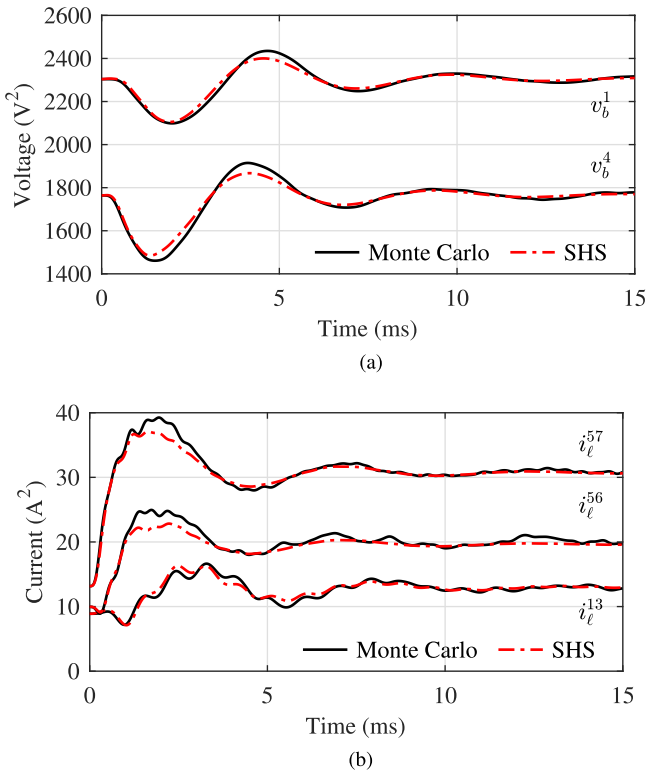

Fig. 9. Comparison of second moment dynamics obtained from Monte Carlo simulations to SHS model predictions. (a) Bus voltage second moments. (b) Line current second moments.

Carlo results are shown as averages over the independent trials on a sample-by-sample basis.

A. Moment Dynamics of $X(t)$

The primary function of the SHS model is to accurately predict the dynamics of moments of system state variables. Comparisons of SHS model predictions to moment dynamics obtained from Monte Carlo simulations are shown in Figs. 8 and 9. The first moments are shown in Fig. 8 for selected bus voltage and line current states. Second order moments are shown in Fig. 9. The figures show that the SHS predictions match Monte Carlo simulations both in transient response and steady-state behavior. Similarly matching plots may be shown for all other system state variables.

B. Moment Dynamics of ZVS Conditions

In addition to state moment dynamics, the SHS model correctly predicts the evolution of moments of ZVS conditions. This is shown for DAB 3 and 4 in Fig. 10. For these converters, the output voltage is always less than the input voltage, and the existence of ZVS is therefore governed by $h_d(x,u)$. Fig. 10 shows comparisons of first and second moments of $h_d(x,u)$ observed in Monte Carlo simulations to SHS model predictions. These results indicate that the SHS framework is capable of accurately predicting the moments of nonlinear algebraic functions of system states and inputs.

The purpose of computing moments of ZVS conditions is to obtain approximate bounds on the probability of ZVS. Fig. 11 shows ZVS probability bounds calculated using (80) and (81). The point of comparison in this case is the relative frequency of ZVS in Monte Carlo simulations. For each trial, a sequence of binary variables is defined according to whether ZVS occurs at each time sample. The average of these sequences indicates the relative frequency of ZVS in simulation.

The results in Fig. 11 show that the tightness of the bound varies for each converter. For instance, the upper bound shown in Fig. 11(a) for DAB 3 is loose in comparison to the lower bound for DAB 5, shown in Fig. 11(c). Fig. 10 indicates the reason for this difference. For DAB 3, the first moment of $h_d(x,u)$ is close to zero. As a result, the tail probability assessed in (80) and (81) is a significant fraction of the overall distribution, and the bound given by the Cantelli inequality is conservative. In contrast, the first moment of $h_d(x,u)$ for DAB 5 is further from zero, and the tail probability is more accurately assessed.

C. Improving ZVS Performance

In addition to predicting ZVS behavior, the SHS model and ZVS condition functions may be used to improve soft-switching performance. A simple example is given here, in which the proportional gain of a voltage controller is adjusted to maximize the probability of ZVS. Fig. 12 shows the ZVS condition equation for a DAB converter in step-down operation. The x and y axes of the plot are phase shift and voltage gain, respectively, and input

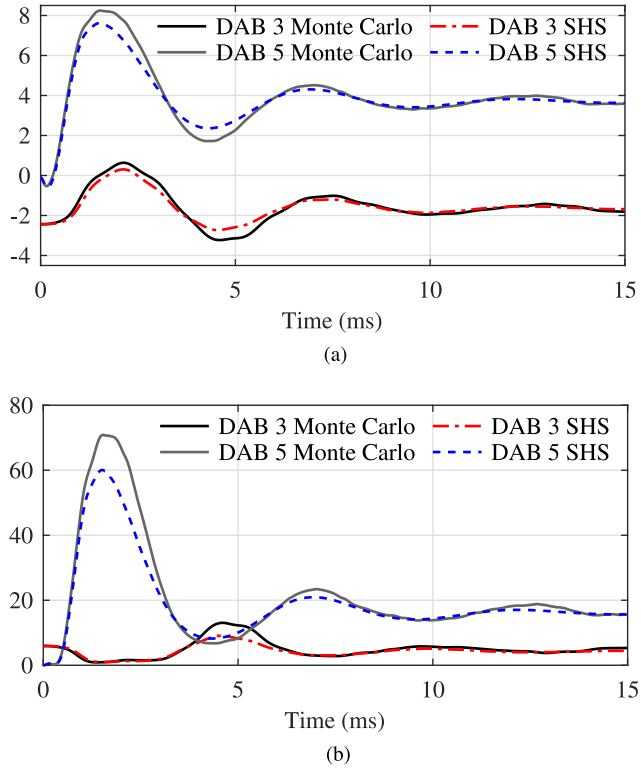

Fig. 10. Comparison of $\mathbb{E}[h_d(x,u)]$ and $\mathbb{E}[(h_d(x,u))^2]$ obtained from Monte Carlo simulations to SHS model predictions. Results are shown for converters 3 and 5. (a) First moment of $h_d(x,u)$. (b) Second moment of $h_d(x,u)$.

voltage is assumed constant. This is a simple way of visualizing ZVS limits: ZVS occurs in all operating points above the limit line. Superimposed on the plot are three steady-state operating points that correspond to three modes of a load process. In this case, each mode is characterized by a different voltage reference and load current.

All three operating points are above the converter's ZVS limit. A steady-state analysis would therefore conclude that this converter always experiences ZVS. In practice, however, transient conditions when transitioning between modes cause the converter to exit the ZVS region. The SHS model is capable of identifying this behavior provides a means for mitigating its effect. The objective in this example is to maximize ZVS probability by changing controller gain. The function to be maximized is then

$$F(\xi, k_p) = \frac{(\xi^{(1)}(t))^2}{\xi^{(2)}(t)}. \tag{82}$$

A simple iterative approach to this maximization is the steepest descent. Since the proportional gain k_p is to be adjusted, the iteration is

$$k_p = k_p + \epsilon \frac{\partial F(\xi, k_p)}{\partial k_p} \tag{83}$$

where ϵ is the step-size parameter, and is small (10^{-4} in this example). This iteration continues until the derivative term in (83) drops below a predetermined threshold. Fig. 13(a) shows the

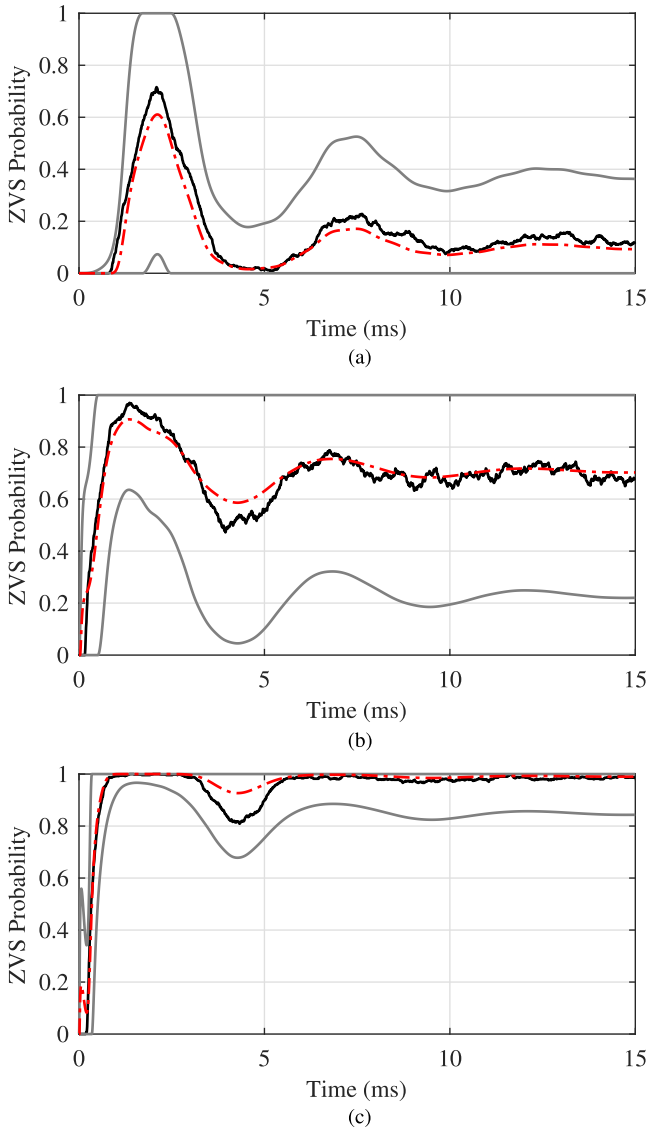

Fig. 11. Comparison of ZVS probability bounds from SHS to results from Monte Carlo simulations. (a) DAB 3 ZVS probability. (b) DAB 4 ZVS probability. (c) DAB 5 ZVS probability.

change in $F(\xi, k_p)$ and k_p over 600 steepest descent iterations. The initial value of k_p is 0.01; after 600 iterations, the gain is $k_p = 0.0402$. Fig. 13(b) shows the results of Monte Carlo simulations before and after tuning the controller gain. These results clearly show the improvement in ZVS performance due to the gain adjustments.

D. Discussion of Results

Monte Carlo simulation is the most common approach to predicting expected microgrid behavior with uncertain load influences. This is why Monte Carlo results are the point of comparison for verification experiments. The advantage of Monte Carlo analysis is simplicity. If a deterministic dynamic model is already available, the main difficulty is specifying parameters of the stochastic influences on the system. The disadvantage is computational efficiency. The execution time of a single

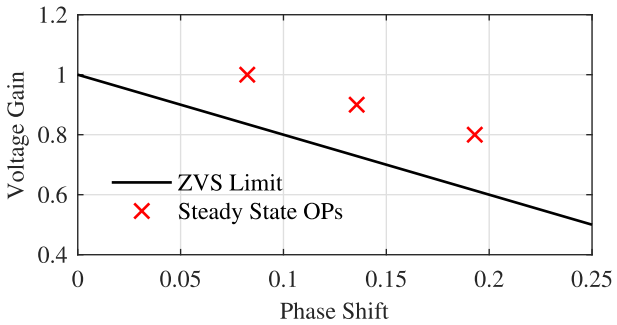

Fig. 12. Step-down ZVS limit and operating points for a three-mode load process.

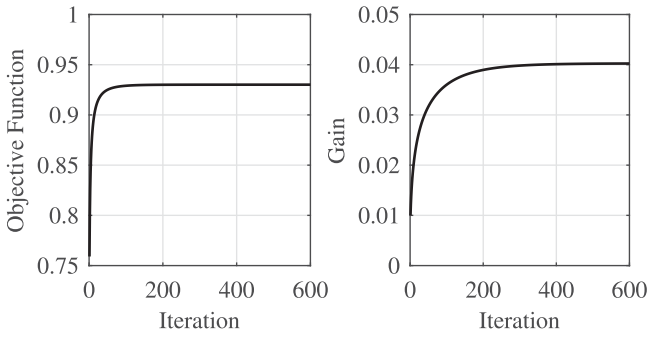

(a)

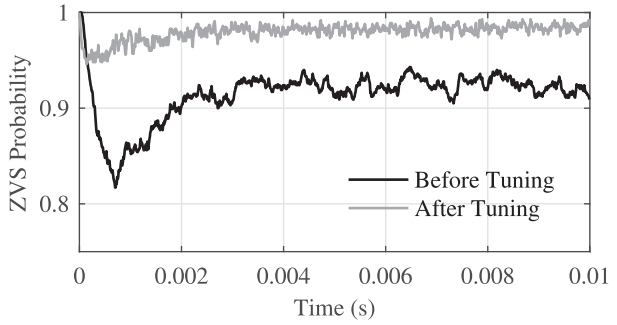

(b)

Fig. 13. Maximization of ZVS probability using steepest descent on proportional gain parameter. (a) Changes in gain and objective function over 600 iterations. (b) ZVS probability before and after tuning k_p.

nonlinear simulation scales with system complexity and error tolerance. The accuracy of the final analysis depends on the number of simulations performed. If the system complexity is too great, or if a wide variety of operating conditions must be analyzed, accurate Monte Carlo simulations become either too time consuming or resource intensive to be useful.

In contrast, the SHS framework and proposed modeling algorithms are more complicated, but once the model is constructed the moment computations are highly efficient. For the seven-bus system, computing all low order moments was significantly faster than a single simulation performed as part of the Monte Carlo analysis. This is a significant benefit in terms of usability. More importantly, it allows the SHS model to be applied to both analysis and design. The iterative optimization of ZVS performance demonstrates how the SHS model and moment calculations may be applied to a design challenge. Because of the number of iterations involved in the optimization, it would be impractical to use Monte Carlo simulations for this purpose.

VI. Conclusion

This article presents two contributions. The first is a method of predicting the influence of random load behavior on dc microgrids and distribution systems. At the core of this method is a stochastic process that represents the combined behavior of loads throughout the system. The model that governs the load process is constructed from individual device models, which are trained using simple parameter estimation algorithms. Using the SHS framework, the load process is combined with deterministic system-level models. The resulting SHS model provides the tools necessary to analyze the effects of load behavior on system dynamics.

The second contribution is a method of assessing the probability of ZVS in DAB converters for a given set of load devices. ZVS conditions are encoded as a function of dynamic state moments. Leveraging the functionality of the SHS model, moments of the ZVS condition functions are obtained. These moments are used in Cantelli's inequality to produce a set of bounds on ZVS probability. While the proposed method of ZVS assessment is specific to the DAB topology, it represents an example of how desirable operating conditions may be represented in the SHS model.

Acknowledgment

Sandia National Laboratories is a multimission laboratory managed and operated by the National Technology and Engineering Solutions of Sandia, LLC, a wholly owned subsidiary of Honeywell International Inc., for the U.S. Department of Energy's National Nuclear Security Administration under contract DE-NA0003525. This article describes objective technical results and analysis. Any subjective views or opinions that might be expressed in the article do not necessarily represent the views of the U.S. Department of Energy or the United States Government.

References

[1] R. H. Lasseter, "Microgrids," in *Proc. IEEE Power Eng. Soc. Winter Meeting*, vol. 1, 2002, pp. 305–308.
[2] T. Dragičević, X. Lu, J. C. Vasquez, and J. M. Guerrero, "Dc microgrids part ii: A review of power architectures, applications, and standardization issues," *IEEE Trans. Power Electron.*, vol. 31, no. 5, pp. 3528–3549, May 2016.
[3] A. T. Elsayed, A. A. Mohamed, and O. A. Mohammed, "Dc microgrids and distribution systems: An overview," *Electric Power Syst. Res.*, vol. 119, pp. 407–417, 2015.
[4] B. Zahedi and L. E. Norum, "Modeling and simulation of all-electric ships with low-voltage dc hybrid power systems," *IEEE Trans. Power Electron.*, vol. 28, no. 10, pp. 4525–4537, Oct. 2013.
[5] P. Kundur, N. J. Balu, and M. G. Lauby, *Power System Stability and Control, Ser. EPRI Power System Engineering Series*. New York: McGraw-Hill, 1994.
[6] H. Wang, M. Liserre, and F. Blaabjerg, "Toward reliable power electronics: Challenges, design tools, and opportunities," *IEEE Ind. Electron. Mag.*, vol. 7, no. 2, pp. 17–26, Jun. 2013.
[7] G. Gross and F. D. Galiana, "Short-term load forecasting," *Proc. IEEE*, vol. 75, no. 12, pp. 1558–1573, 1987.

[8] M. T. Hagan and S. M. Behr, "The time series approach to short term load forecasting," *IEEE Trans. Power Syst.*, vol. 2, no. 3, pp. 785–791, Aug. 1987.
[9] B. Hajek, *Random Processes for Engineers*. Cambridge: Cambridge University Press, 2015.
[10] A. Papoulis, *Probability, Random Variables, and Stochastic Processes, 3rd ed., McGraw-Hill Series in Electrical Engineering Communications and Signal Processing*. New York, NY, USA: McGraw-Hill, 1991.
[11] A. Marinescu, C. Harris, I. Dusparic, S. Clarke, and V. Cahill, "Residential electrical demand forecasting in very small scale: An evaluation of forecasting methods," in *Proc. 2nd Int. Workshop Softw. Eng. Challenges Smart Grid*, 2013, pp. 25–32.
[12] G. Hart, "Nonintrusive appliance load monitoring," *Proc. IEEE*, vol. 80, no. 12, pp. 1870–1891, Dec. 1992.
[13] F. Sultanem, "Using appliance signatures for monitoring residential loads at meter panel level," *IEEE Trans. Power Del.*, vol. 6, no. 4, pp. 1380–1385, Oct. 1991.
[14] A. Zoha, A. Gluhak, M. Nati, and M. Imran, "Low-power appliance monitoring using factorial hidden Markov models," in *Proc. 8th Int. Conf. Intell. Sensors Sensor Netw. Inf. Process.*, Apr. 2013, pp. 527–532.
[15] T. Zia, D. Bruckner, and A. Zaidi, "A hidden Markov model based procedure for identifying household electric loads," in *Proc. 37th Conf. Ind. Electron.*, Nov. 2011, pp. 3218–3223.
[16] S. Makonin, F. Popowich, I. Bajic, B. Gill, and L. Bartram, "Exploiting HMM sparsity to perform online real-time nonintrusive load monitoring," *IEEE Trans. Smart Grid*, vol. 7, no. 6, pp. 2575–2585, Nov. 2016.
[17] J. A. Mueller and J. W. Kimball, "Accurate energy use estimation for nonintrusive load monitoring in systems of known devices," *IEEE Trans. Smart Grid*, vol. 9, no. 4, pp. 2797 –2808, Jul. 2018.
[18] A. Alghassi, S. Perinpanayagam, M. Samie, and T. Sreenuch, "Computationally efficient, real-time, and embeddable prognostic techniques for power electronics," *IEEE Trans. Power Electron.*, vol. 30, no. 5, pp. 2623–2634, May 2015.
[19] Y. Cao, J. A. Magerko, T. Navidi, and P. T. Krein, "Power electronics implementation of dynamic thermal inertia to offset stochastic solar resources in low-energy buildings," *IEEE Trans. Emerg. Sel. Topics Power Electron.*, vol. 4, no. 4, pp. 1430–1441, Dec. 2016.
[20] M. Milton, C. A. De La O, H. L. Ginn, and A. Benigni, "Controller-embeddable probabilistic real-time digital twins for power electronic converter diagnostics," *IEEE Trans. Power Electron.*, vol. 35, no. 9, pp. 9850–9864, Sep. 2020.
[21] Q. Su and K. Strunz, "Stochastic polynomial-chaos-based average modeling of power electronic systems," *IEEE Trans. Power Electron.*, vol. 26, no. 4, pp. 1167–1171, Apr. 2011.
[22] P. Manfredi, I. S. Stievano, and F. G. Canavero, "Stochastic analysis of switching power converters via deterministic SPICE equivalents," *IEEE Trans. Power Electron.*, vol. 29, no. 9, pp. 4475–4478, Sep. 2014.
[23] J. P. Hespanha, "Modelling and analysis of stochastic hybrid systems," *IEE Proc. - Control Theory Appl.*, vol. 153, no. 5, pp. 520–535, 2006.
[24] S. V. Dhople, Y. C. Chen, L. DeVille, and A. D. Domínguez-García, "Analysis of power system dynamics subject to stochastic power injections," *IEEE Trans. Circuits Syst. I*, vol. 60, no. 12, pp. 3341–3353, Dec. 2013.
[25] G. Mpembele and J. Kimball, "Analysis of a standalone microgrid stability using generic Markov jump linear systems," in *Proc. IEEE Power Energy Conf. Illinois*, 2017, pp. 1–8.
[26] J. A. Mueller and J. W. Kimball, "Analysis of soft-switching performance for a dc-dc dual active bridge converter with randomly varying loads," in *Proc. IEEE Energy Convers. Congr. Expo.*, Sep. 2018, pp. 4246–4253.
[27] G. Pola, M. L. Bujorianu, J. Lygeros, and M. D. DiBenedetto, "Stochastic hybrid models: An overview," *IFAC Proc. Volumes*, vol. 36, no. 6, pp. 45–50, 2003.
[28] J. A. Mueller and J. W. Kimball, "Modeling dual active bridge converters in dc distribution systems," *IEEE Trans. Power Electron.*, vol. 34, no. 6, pp. 5867–5879, Jun. 2019.
[29] A. Emadi, "Modeling and analysis of multiconverter dc power electronic systems using the generalized state-space averaging method," *IEEE Trans. Ind. Electron.*, vol. 51, no. 3, pp. 661–668, Jun. 2004.
[30] J. A. Mueller and J. Kimball, "An improved generalized average model of dc-dc dual active bridge converters," *IEEE Trans. Power Electron.*, vol. 33, no. 11, pp. 9975–9988, Nov. 2018.
[31] M. N. Kheraluwala, R. W. Gascoigne, D. M. Divan, and E. D. Baumann, "Performance characterization of a high-power dual active bridge dc-to-dc converter," *IEEE Trans. Ind. Appl.*, vol. 28, no. 6, pp. 1294–1301, Nov./Dec. 1992.
[32] A. Rodríguez, A. Vázquez, D. G. Lamar, M. M. Hernando, and J. Sebastián, "Different purpose design strategies and techniques to improve the performance of a dual active bridge with phase-shift control," *IEEE Trans. Power Electron.*, vol. 30, no. 2, pp. 790–804, Feb. 2015.
[33] R. T. Naayagi, A. J. Forsyth, and R. Shuttleworth, "High-power bidirectional dc-dc converter for aerospace applications," *IEEE Trans. Power Electron.*, vol. 27, no. 11, pp. 4366–4379, Nov. 2012.
[34] I. R. Savage, "Probability inequalities of the Tchebycheff type," *J. Res. Nat. Bur. Standards*, vol. 65B, no. 3, pp. 211–226, 1961.

Jacob A. Mueller (Member, IEEE) received the B.S., M.S., and Ph.D. degrees in electrical engineering from Missouri University of Science and Technology, Rolla, MO, USA, in 2012, 2014, and 2018, respectively.

Since 2018, he has been with the Energy Storage Technology and Systems Department at Sandia National Laboratories, Albuquerque, NM, USA, where he is currently Senior Member of Technical Staff. His research interests include modeling and control of power electronics, dc microgrids, and power conversion systems for utility-scale energy storage applications.

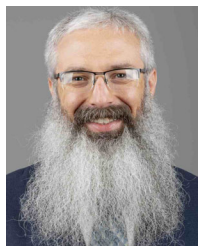

Jonathan W. Kimball (Senior Member, IEEE) received the B.S. degree in electrical and computer engineering from Carnegie Mellon University, Pittsburgh, PA, USA, in 1994, and the M.S. degree in electrical engineering and the Ph.D. degree in electrical and computer engineering from the University of Illinois at Urbana-Champaign, Illinois, USA, in 1996 and 2007, respectively.

From 1996 to 1998, he worked with Motorola, Phoenix, AZ, USA, designing IGBT modules for industrial applications. He then joined Baldor Electric, Fort Smith, AR, USA, where he designed industrial adjustable speed drives ranging 1–150 hp. In 2003, he returned to the University of Illinois at Urbana-Champaign, as a Research Engineer and later a Senior Research Engineer. Later in 2003, he cofounded SmartSpark Energy Systems, Inc., in Champaign, IL, USA, and served as Vice President of Engineering. In 2008, he joined as an Assistant Professor with the Faculty of Missouri S&T (formerly the University of Missouri-Rolla), where he was promoted to an Associate Professor in 2014, and to a Professor of electrical and computer engineering in 2018. From 2016 to 2018, he was also a Dean's Scholar of the College of Engineering and Computing. Since 2019, he has been serving as the Interim Director of the Missouri S&T Center for Research in Energy and the Environment. His research interests include microgrids, switched-capacitor converters, and cyber-physical systems.

Dr. Kimball is a member of Eta Kappa Nu, Tau Beta Pi, and Phi Kappa Phi. He is a Senior Member of the Institute of Electrical and Electronics Engineers (IEEE). He is a Licensed Professional Engineer in the State of Illinois. He was the General Chair of the IEEE Applied Power Electronics Conference in 2017 and continues to serve on its steering committee.